# Microscopic Studies on Liquid Crystal Poly(3,3‴-dialkylquaterthiophene) Semiconductor

**Ni Zhao, Gianluigi A. Botton,* Shiping Zhu, and Andy Duft**

*Department of Materials Science and Engineering, McMaster University, Hamilton, Ontario, Canada L8S4L7*

**Beng S. Ong,* Yiliang Wu, and Ping Liu**

*Materials Design and Integration Laboratory, Xerox Research Center of Canada, Mississauga, Ontario, Canada L5K2L1*

*Received July 29, 2004; Revised Manuscript Received August 19, 2004*

ABSTRACT: Through tapping mode atomic force microscopy and transmission electron microscopy, we were able to directly visualize the nature of crystal domains of liquid crystalline poly(3,3‴-dialkylquaterthiophene) in its spin-coated films. The size of domains, consisting of large anisotropic lamellar stacks formed by arrays of $\pi-\pi$ stacking polymer chains, was highly dependent on annealing temperature covering the range from the crystal-to-liquid crystal to the liquid crystal-to-isotropic phase transitions. After annealing at the melting temperature, slow cooling gave rise to close packing of parallel lamellar stacks within the domain, while fast cooling led to clear separation of lamellar stacks. The surface modification of the substrate was particularly critical to the orientation of these domains of lamellar stacks: the $SiO_2$-surface modified with octyltrichlorosilane led to lamellar stacking domains oriented with their lamellar axes normal to the modified surface.

## Introduction

Recently, organic field effect transistors (OFETs) have been intensively studied for potential use in low-cost, large-area, and flexible electronic devices (e.g., active matrix displays).[1−10] The performance of these devices crucially depends on the structural order of the semiconductor molecules, as properly ordered structures have been shown to lead to high charge carrier mobility.[1,3,8] For example, pentacene films with different phases and morphologies have been fabricated under various processing conditions (e.g., deposition temperature, substrate surface properties, etc.), which result in a wide range of mobility.[1,11,12] However, pentacene is an insoluble material and requires vacuum deposition to fabricate semiconductor layers for OFETs. On the other hand, regioregular polythiophenes are soluble in common organic solvents and have been satisfactorily solution-processed into OFET semiconductor layers. Certain regioregular polythiophenes have also exhibited a strong tendency to self-organize into highly ordered structures as revealed by X-ray and STM studies.[8,13] However, the thin-film morphologies and the effects of processing conditions on thin-film formation of polythiophenes have not been extensively studied as in the case of pentacene. The information and knowledge needed to improve the performance of polythiophene-based OFETs through processing conditions are therefore still lacking.

Recently, a new class of solution-processable high-performance polythiophene, poly(3,3‴-dialkylquaterthiophene) (PQT) (Figure 1a), with a mobility up to 0.1−0.2 $cm^2\ V^{-1}\ s^{-1}$ was reported.[14] Properly conditioned thin films of PQT showed the presence of extensive crystalline domains consisting of both the $\pi-\pi$ and the interlayer stacking of backbones, with an additional ordering from side chain interdigitation (Figure 1b). Compared to other regioregular poly(3-alkylthiophene)s (PATs) such as poly(3-hexylthiophene) (P3HT), PQT possessed higher air stability, which enabled its fabrication into a high-mobility semiconductor layer via solution deposition under ambient conditions. In addition, PQT also exhibited a liquid crystal phase at a certain temperature range below its melting point.[14] This makes it potentially possible to manipulate its film morphologies to enhance device performance through external forces, as demonstrated for some liquid crystalline polymers such as poly-9,9′-dioctylfluorene-*co*-bithiophene (F8T2).[9]

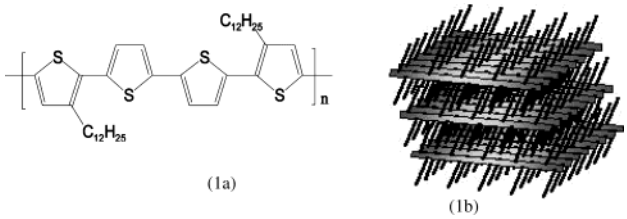


**Figure 1.** (a) Molecular structure of PQT; (b) 3D packing of PQT molecules.

The crystal structure of PQT films has been studied by X-ray diffraction (XRD),[14] and the temperature dependence of molecular packing of the PAT family polymers has been well modeled.[15,16] These results are, however, an average over volume that might contain different phase components. The studies of surface morphology of PQT films by microscopy may lead to a better understanding of the nature of its molecular organization. Unlike traditional liquid crystals, PQT is an inverse comblike polymer that does not generally form large-sized liquid crystal domains. While the largest domains of PQT were at submicron levels and were visible under polarized optical microscope, no details related to fine structures within the domain

* Corresponding authors. G. Botton: Ph 1-905-525-9140 ext 24767; e-mail gbotton@mcmaster.ca. B. Ong: Ph 1-905-823-7091 ext 459; e-mail Beng.Ong@crt.xerox.com.

10.1021/ma048434s CCC: $27.50 
Published on Web 10/01/2004

could, however, be obtained. In this work, we show that the structure and morphology of nanosized liquid crystal domains of PQT could be clearly visualized and understood using the tapping mode AFM combined with transmission electron microscopy (TEM). We present here the successful imaging of both the surface texture and the 3D structure of a highly structured polythiophene semiconductor layer of PQT. Systematic AFM studies of PQT films with the objective of elucidating the effects of annealing conditions, phase transition, and surface modification on film morphology will also be discussed herein.

## Experimental Section

**Materials and Sample Preparation.** PQT was synthesized by $FeCl_3$-mediated oxidative coupling polymerization.[14] The molecular weight and distribution ($M_n$ = 17 300 and $M_w/M_n$ = 1.32, respectively) were determined by gel permeation chromatography (GPC) using polystyrene as a standard. The absolute molecular weight was also measured by matrix-assisted laser desorption ionization-mass spectrometry (MALDI-MS) to be 5323−6647. The thermal characteristics of PQT were studied using a differential scanning calorimeter (DSC) (TA-DSC2910) with a scanning rate of 10 °C/min. AFM samples were made with the same configuration as top-contact OFETs without the source and drain electrodes present. An $n^+$-Si wafer with 100 nm $SiO_2$ layer was used as the substrate which was pretreated with 0.1 M octyltrichlorosilane (OTS8) solution at 60 °C for 20 min to grow a silane self-assembled monolayer. PQT films were spin-coated from 0.3 wt % polythiophene nanoparticle dispersion[17] at a speed of 1000 rpm using dichlorobenzene as a solvent and then vacuum-dried for 2 h. The film thickness was around 30−50 nm. Annealing was carried out at the temperatures showing different phase transitions as revealed in the DSC scans. Details of annealing conditions are provided with the reported AFM images.

TEM samples were spin-coated from 0.2 wt % polythiophene solution at a speed of 2000 rpm on freshly cleaved mica and vacuum-annealed at 150 °C for 15 min. Mica was used here as the substrate because it has similar surface chemistry (i.e., −OH groups) as that of $SiO_2$. The PQT films were subsequently delaminated from the mica by dipping the samples into water and transferred onto 500 mesh TEM copper grids for electron microscopy studies.

**AFM and TEM Procedures.** The AFM experiments were performed with a Nanoscope IIIa MultiMode scanning probe microscope (Digital Instruments) operated at ambient conditions. Si tips with a resonance frequency of approximately 300 kHz and a scan rate of 1 Hz were used. All AFM measurements were done in the tapping mode, which enables acquisition of topographical and phase images at the same time. Phase images are especially useful for direct visualization of our PQT samples. The contrast in phase images comes from the phase shift of the oscillating cantilever relative to the driving signal when it interacts with the samples. The phase contrast essentially arises from the difference of energy dissipation during tip−sample interaction. This enables it to differentiate between areas with different viscoelastic properties.[18−20] In the phase image of crystallized polymer films, the less energy dissipative feature like crystalline phase appears brighter, while the amorphous phase appears darker. TEM imaging was performed using a Philips CM12 at an accelerating voltage of 120 kV. The phase structure was revealed by operating the microscope at a relatively strong underfocus condition in order to increase the image contrast, as discussed in ref 21.

## Results and Discussion

**1. Imaging of Film Morphology.** Figure 2 presents the AFM images of (a) topography and (b) phase acquired simultaneously on the PQT film which was annealed at 148 °C. The surface roughness of the film

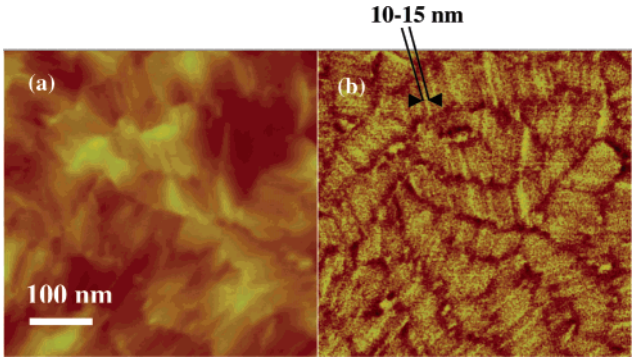


**Figure 2.** AFM (a) topographic and (b) phase images of PQT films deposited on OTS8-modified substrates. Films were annealed at 148 °C for 15 min and cooled in a vacuum.

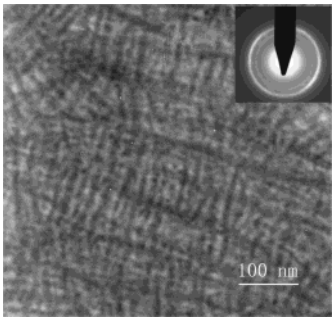


**Figure 3.** TEM image and selected area diffraction pattern of PQT free-standing films after annealing.

could be directly measured from the topographic image to be about 1.1 nm. The phase image was highly informative as it clearly showed PQT crystal domains with parallel lamellar structures. Each "lamella" was approximately 10−15 nm wide, which corresponds to the length of the polymer backbones. This suggests that one "lamella" is actually an array of $\pi-\pi$ stacked polymers (Figure 1b) and that regions of closely packed lamellae form larger domains.

Similar features can be observed in the TEM image of a free-standing film of PQT (Figure 3). The TEM data supported that the lamellar stacks shown in the phase image (Figure 2b) were representative of the structure throughout the entire film thickness instead of just at the surface. Moreover, the only ring visible in the selected area diffraction pattern of the thin film at around 3.7−3.8 Å corresponds to the $\pi-\pi$ stacking distance. This directly indicates the in-plane orientation of the $\pi-\pi$ stacking and supports our previous model for the lamella stacking. However, several differences between TEM and AFM images were observed. Since the TEM image is in essence a projection from a 3D structure, if a domain does not extend through the thickness of the film, overlapping of misoriented domains within the film thickness will occur and intersecting features will appear in the images. The apparently larger width of each lamella in the TEM image is due to the broadening of features at the large underfocus condition. The domain sizes are also different in the TEM images as compared to AFM, possibly due to the use of different substrates. Nevertheless, the TEM image strongly supports the fact that the texture we observed by AFM was representative of the entire film structure throughout its thickness. Since the AFM images showed the domain morphology more clearly and more readily on devices of interest, we therefore conducted our morphology studies using the AFM.

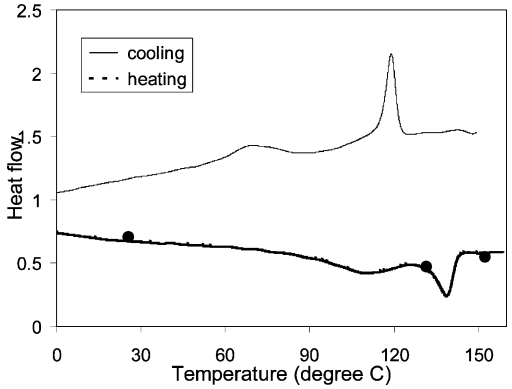


**Figure 4.** DSC thermogram (circles in the heating curve indicate the temperatures corresponding to the quench experiment).

**2. Film Morphology in Different Phases.** The DSC thermogram (Figure 4) shows two endotherms at 110 and 140 °C (at peak value) on heating, corresponding respectively to crystal-to-liquid crystal and liquid crystal-to-isotropic phase transitions. The morphologies of films in different phases are presented in Figure 5. After spin-coating, all the film samples were annealed at 148 °C for 15 min and cooled in a vacuum. This pretreatment of annealing above the liquid crystal-to-isotropic phase transition temperature and slow cooling in a vacuum assured a well-developed crystal domain structure as shown in Figure 5a. The films were then reheated to two different temperatures (133 and 155 °C) for 30 min and quenched in liquid nitrogen. The rapid cooling by quenching retained the film morphology of the annealing temperature. The objective of this experiment was to examine the effects of a possible materials postprocessing procedure on the well-developed crystal domain structure. The sample that was quenched from the liquid crystal phase at 133 °C (Figure 5b) showed very similar texture as the crystal phase (Figure 5a). However, when the temperature went beyond the melting peak, the long-range ordering disappeared (Figure 5c).

The results can be interpreted and correlated with the temperature-controlled XRD data of regioregular polythiophenes with long side chains,[15,16] which have similar molecular structure as PQT. The XRD results showed that the phase transition from crystal to liquid crystal only involved the melting and disordering of side chains, while the backbone stacking remained an ordered structure. Our results (Figure 5a,b) further revealed that losing the side-chain ordering did not cause significant changes in morphology. This effect suggests that the texture of the liquid crystal phase was retained in the crystal phase during cooling. This is a significant property for film fabrication of OFETs as it shows that the $\pi-\pi$ stacking of the PQT molecules in the liquid crystal phase could be maintained during cooling to room temperature, resulting in the formation of a crystalline film. This property also allows the possible development of postprocessing procedures of this material in order to realize an alignment of the crystal domains through external forces.

**3. Effect of Annealing Temperature and Cooling Rate on Film Morphology.** Figure 6 shows the AFM topographic and phase images of PQT film samples before and after annealing at various temperatures. These films were freshly spin-coated before annealed for 15 min and cooled in a vacuum overnight. The slow cooling rate in a vacuum allowed the film morphology to be fully developed from the annealing temperature. The mosaic crystal domains started to form when the annealing temperature was in the range of the crystal-to-liquid crystal phase transition (~110 °C). As the temperature increased to 133 °C, the domains size increased anisotropically to the submicron range along the long dimension.

When spun from solution, PQT molecules exhibited a great tendency to form $\pi-\pi$ stacking in view of their intrinsically excellent self-organization capability.[14] However, because of the competition between the crystallization and substrate pulling, only nanosized crystallites containing a small number of stacked molecules were formed (Figure 6a). At the crystal-to-liquid crystal phase transition temperature above 110 °C when the mobility of the molecules is substantially greater, the reorganization of the $\pi-\pi$ stacking arrays occurred, leading to the formation of mosaic crystal domains (Figure 6b,c). Increasing the temperature up to the melting region (at 148 °C) disrupted the $\pi-\pi$ stacking between polymer backbones and completely relaxed the molecules; the polymer molecules were thus able to rearrange to form long-range ordered $\pi-\pi$ stacking structure (Figure 6d) upon slow cooling to room temperature overnight. This ability to form long-range order allowed adequate morphological development.

The film morphology could also be affected by the rate of cooling after annealing. Figure 7 shows the topographic and phase images of the PQT film annealed at 148 °C for 15 min. The cooling rate with constant nitrogen gas blowing on the sample's surface was faster than the vacuum cooling (3 h vs overnight). This fast cooling yielded a clear separation between the lamellar stacks (Figure 7), in contrast to slow cooling that produced a well-developed crystal domain structure (Figure 6d). This observation was consistent with our previous discussion on the film morphology in different phases. When fast cooling was applied to the partially

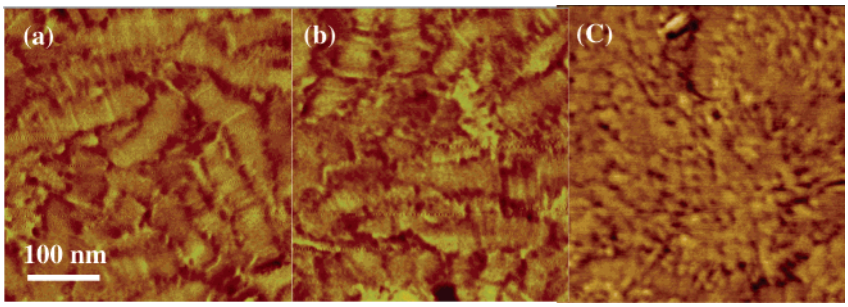


**Figure 5.** Phase images of PQT films deposited on OTS8 modified substrates. Films were annealed at (a) 148 °C for 15 min and cooled in a vacuum. The films were then reheated to (b) 133 and (c) 155 °C respectively for 30 min and quenched in liquid nitrogen.

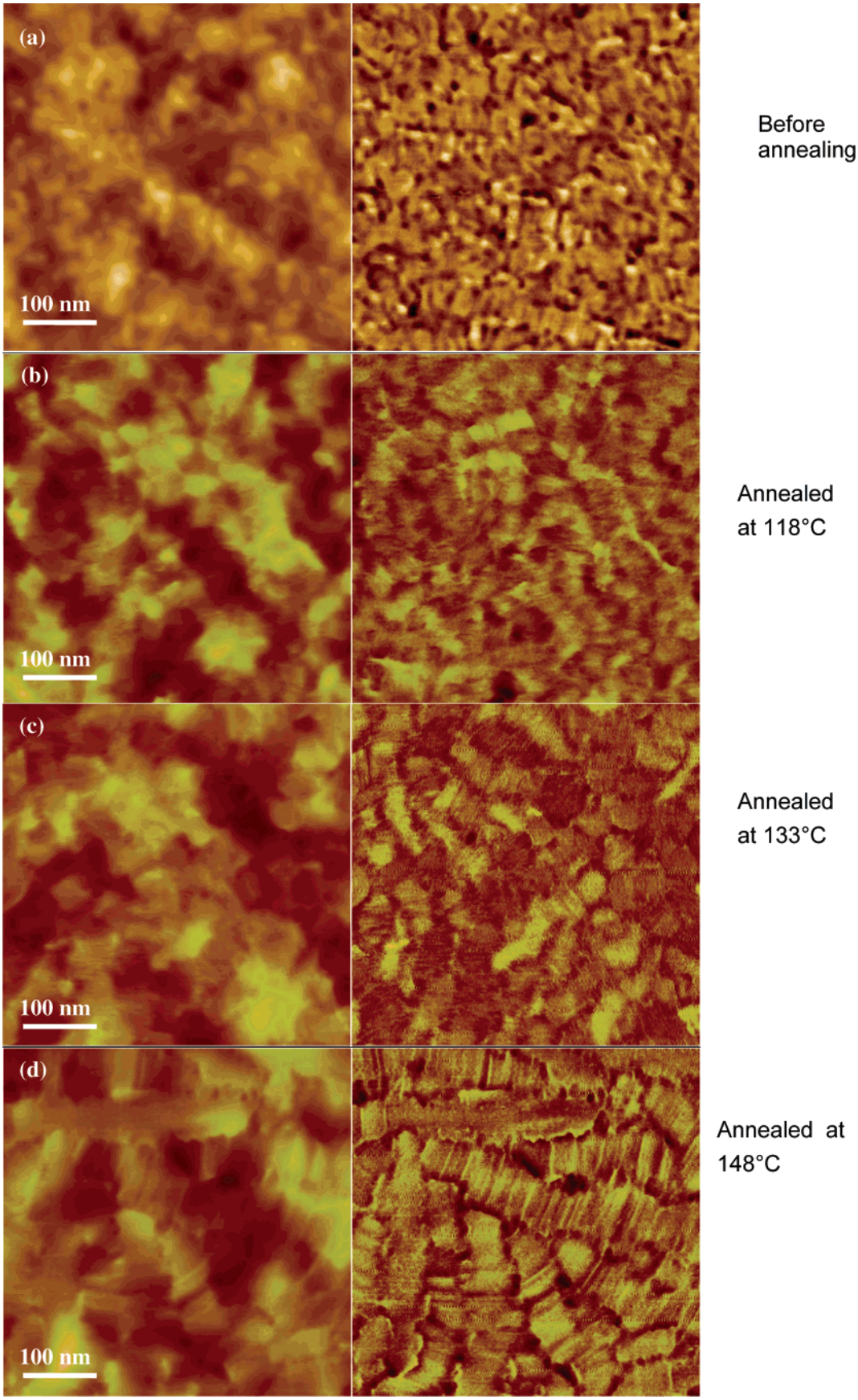


**Figure 6.** AFM topographic (left column) and phase (right column) images of PQT films deposited on OTS8-modified substrates. The morphology of the films before annealing is revealed in (a). Films were annealed at (b) 118, (c) 133, and (d) 148 °C for 15 min and cooled in a vacuum overnight.

melted PQT film annealed at 148 °C, visible loss in the long-range ordering was observed. The fast cooling from the amorphous state resulted in the incomplete transformation to liquid crystal state. This result indicated

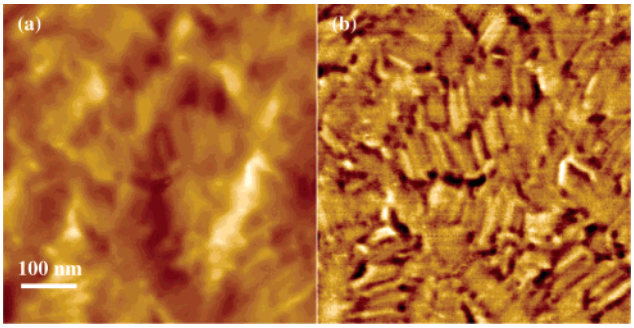


**Figure 7.** AFM (a) topographic and (b) phase images of PQT film deposited on OTS8-modified substrate. The film was annealed at 148 °C for 15 min. Constant nitrogen gas flow was blown on the sample's surface to control the cooling rate. The cooling procedure took approximately 3 h from annealing to room temperature.

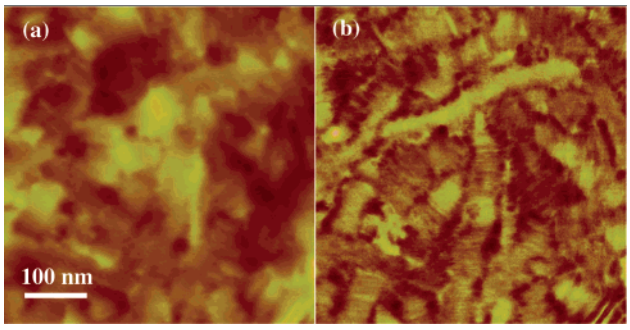


**Figure 8.** AFM (a) topographic and (b) phase images of PQT film deposited on unmodified substrates. Films were annealed at 148 °C for 15 min and cooled in a vacuum.

that cooling conditions following annealing at the melting temperature have a decisive influence on the molecular ordering and thus film morphology of PQT films.

**4. Effect of Substrate on Film Morphology.** It has been reported that the surface properties of insulator layers have a significant effect on the electrical properties of polymer semiconductors.[3,22] Here we studied the role of the surface modification on the film morphology. The phase image of the film deposited on an untreated $SiO_2$ surface (Figure 8) shows a similar lamellar stacking structure as the one in the film deposited on OTS8-modified substrates (Figure 6d). This indicated that the 3D crystal structure was not affected by the surface modification. However, the domains on the untreated $SiO_2$ substrate in Figure 8 were smaller in size with relatively nonuniform size distribution as compared to Figure 6d. In addition, the domains in Figure 8 have different brightness. The origin of this contrast has not been fully understood yet. This effect might be due to different arrangement of the domains and their orientation through the film. This result suggest that the *n*-octyl groups of OTS-8 monolayer help direct the ordering of lamellar stacks such that the $\pi-\pi$ stacking become oriented parallel to the modified surface. The studies on the effect of OTS8 on OFET performance will be discussed in a subsequent paper.

## Conclusion

Through tapping-mode AFM and TEM, we have shown that the annealed PQT films were highly structured in nature and contain anisotropic crystalline domains of parallel lamellae of $\pi-\pi$ stacking PQT polymer chains. The nature of the crystalline domains and lamellar ordering were critically dependent on the annealing and cooling conditions. The crystal domains in PQT films were essentially similar to those of its liquid crystals when the film was annealed at the crystal-to-liquid crystal temperature range. Annealing at the melting temperature resulted in the formation of significantly different domain order depending on the rate of cooling: fast cooling led to domains with clearly separated lamellae with amorphous order or gaps between them during rapid solidification, while slow cooling resulted into well packed lamellae with much less amorphous regions. In addition, OTS-8 modified surface was found to exert a definitive influence on the orientation of PQT lamellae such that the $\pi-\pi$ stacking were oriented parallel to the surface.

**Acknowledgment.** We thank the Natural Science and Engineering Research Council of Canada (NSERC) and the Xerox Foundation for supporting this research. We also thank the Canada Foundation of Innovation (CFI), the Ontario Innovation Trust, and Xerox Research Center of Canada (XRCC) for supporting the research facilities.

## References and Notes

(1) Dimitrakopoulos, C. D.; Mascaro, D. J. *Adv. Mater.* **2002**, *14*, 99−117.
(2) Garnier, F.; Hajlaoui, R.; Yassar, A.; Srivastava, P. *Science* **1994**, *265*, 1684−1686.
(3) (a) Sirringhaus, H.; Tessler, N.; Friend, R. H. *Science* **1998**, *280*, 1741−1744. (b) Sirringhaus, H.; Brown, P. J.; Friend, R. H.; Nielen, M. M.; Bechgaard, K.; Langeveld-Voss, B. M. W.; Spiering, A. J. H.; Janssen, R. A. J.; Meijer, E. W.; Herwig, P.; de Leeuw, D. M. *Nature (London)* **1999**, *401*, 685−688.
(4) Bao, Z. *Adv. Mater.* **2000**, *12*, 227−230.
(5) (a) Gelinck, G. H.; Geuns, T. C. T.; de Leeuw, D. M. *Appl. Phys. Lett.* **2000**, *77*, 1487−1489. (b) Huitena, H. E. A.; Gelinck, G. H.; van der Putter, J. B. P. H.; Kuijk, K. E.; Hart, C. M.; Cantatore, E.; Herwig, P. T.; van Breemen, A. J. J. M.; de Leeuw, D. M. *Nature (London)* **2001**, *414*, 599. (c) Gelinck, G. H.; Huitema, H. E. A.; Van Veenendaal, E.; Cantatore, E.; Schrijnemakers, L.; Van der Putten, J. B. P. H.; Geuns, T. C. T.; Beenhakkers, M.; Giesbers, J. B.; Huisman, B. H.; Meijer, E. J.; Benito, E. M.; Touwslager, F. J.; Marsman, A. W.; Van Rens, B. J. E.; De Leeuw, D. M. *Nature Mater.* **2004**, *3*, 106−110.
(6) (a) Wisnieff, R. *Nature (London)* **1998**, *394*, 225−227. (b) Dimitrakopoulos, C. D.; Purushothaman, S.; Kymissis, J.; Callegari, A.; Shaw, J. M. *Science* **1999**, *283*, 822−824.
(7) (a) Bao, Z.; Feng, Y.; Dodabalapur, A. *Chem. Mater.* **1997**, *9*, 1299−1301. (b) Sirringhaus, H.; Kawase, T.; Friend, R. H.; Shimoda, T.; Inbasekaran, M.; Wu, W.; Woo, E. P. *Science* **2000**, *290*, 2123−2126.
(8) Bao, Z.; Dodabalapur, A.; Lovinger, A. J. *Appl. Phys. Lett.* **1996**, *69*, 4108−4110.
(9) Sirringhaus, H.; Wilson, R. J.; Friend, R. H.; Inbasekaran, M.; Wu, W.; Woo, E. P.; Grell, M.; Bradley, D. D. C. *Appl. Phys. Lett.* **2000**, *77*, 406−408.
(10) Sundar, V. C.; Zaumseil, J.; Podzorov, V.; Menard, E.; Willett, R. L.; Someya, T.; Gershenson, M. E.; Rogers, J. A. *Science* **2004**, *303*, 1644−1646.
(11) Frank-J. Meyer zu Heringdorf, Reuter, M. C.; Tromp, R. M. *Nature (London)* **2001**, *412*, 517−520.
(12) Knipp, D.; Street, R. A.; Volkel, A.; Ho, J. *J. Appl. Phys.* **2003**, *93*, 347−355.
(13) Grevin, B.; Rannou, P.; Payerne, R.; Pron, A.; Travers, J. P. *Adv. Mater.* **2003**, *15*, 881−884.
(14) Ong, B.; Wu, Y. L.; Liu, P.; Garden, S. *J. Am. Chem. Soc.* **2004**, *126*, 3378−3379.
(15) Tashiro, K.; Ono, K.; Minagawa, Y.; Kobayashi, K.; Kawai, T.; Yoshino, K. *J. Polym. Sci., Polym. Phys.* **1991**, *29*, 1223−1233.
(16) Prosa, T. J.; Winokur, M. J.; Moulton, J.; Smith, P.; Heeger, A. J. *Macromolecules* **1992**, *25*, 4364−4372.
(17) Ong, B.; Wu, Y. L.; Liu, P.; Garden, S.; Zhao, N.; Botton, G. A., submitted for publication.

(18) Cleveland, J. P.; Anczykowski, B.; Schmid, A. E.; Elings, V. B. *Appl. Phys. Lett.* **1999**, *72*, 2613.
(19) Scott, W. W.; Bhushan, B. *Ultramicroscopy* **2003**, *97*, 151−169.
(20) Marcus, M. S.; Eriksson, M. A.; Darryl, Y. S.; Carpick, R. W. *Ultramicroscopy* **2003**, *97*, 145−150.
(21) Petermann, J.; Gleiter, H. *J. Polym. Sci., Polym. Phys.* **1975**, *13*, 1939−1944.
(22) Salleo, A.; Chabinyc, M. L.; Yang, M. S.; Street, R. A. *Appl. Phys. Lett.* **2002**, *81*, 4383−4385.

MA048434S